Available online at www.sciencedirect.com

SCIENCE DIRECT

Thin Solid Films 480–481 (2005) 118–123

www.elsevier.com/locate/tsf

Structural and chemical investigations of CBD- and PVD-CdS buffer layers and interfaces in Cu(In,Ga)Se_2-based thin film solar cells

D. Abou-Ras[a,b,*], G. Kostorz[a], A. Romeo[b,1], D. Rudmann[b], A.N. Tiwari[b,2]

[a]*ETH Zürich, Institute of Applied Physics, 8093 Zürich, Switzerland*

[b]*ETH Zürich, Thin Film Physics Group, Laboratory for Solid State Physics, Technoparkstrasse 1, 8005 Zürich, Switzerland*

Available online 8 December 2004

Abstract

It is known that high-efficiency thin film solar cells based on Cu(In,Ga)Se_2 (CIGS) can be obtained using CdS buffer layers grown by chemical bath deposition (CBD). The highest efficiencies achieved with CdS buffer layers produced by physical vapor deposition (PVD) are significantly lower. To find reasons for this difference, structural and chemical properties of CBD- and PVD-CdS buffer layers and their interfaces with CIGS were investigated by means of bright-field (BF-TEM), high-resolution (HR-TEM) and energy-filtered transmission electron microscopy (EF-TEM), and also by energy-dispersive X-ray spectroscopy (EDX) and scanning electron microscopy (SEM). PVD-CdS grains were shown to be clearly larger than the CBD-CdS grains. Also, a large defect density was detected at the PVD-CdS/CIGS interface, which is attributed to the larger lattice mismatch than at the CBD-CdS/CIGS interface. Cu diffusion from CIGS into CdS was found for the CBD- and the PVD-CdS sample. The PVD-CdS/CIGS interface turned out to be quite abrupt, whereas the CBD-CdS/CIGS interface is rather diffuse. The differences in efficiencies of solar cells with CBD- and PVD-CdS buffer layers can partly be explained by referring to the higher defect density and the probable absence of an inversion of the near-interface region from p- to n-type at the PVD-CdS/CIGS interface.

© 2004 Elsevier B.V. All rights reserved.

Keywords: Physical vapor deposition; Chemical bath deposition; CdS buffer

1. Introduction

The highest efficiencies for thin film solar cells based on a Cu(In,Ga)Se_2 (CIGS) and $CuInSe_2$ (CIS) absorber layers have been achieved using a CdS buffer layer deposited by a chemical bath deposition (CBD) process. A typical CBD solution consists of dissolved Cd^{2+} ions, thiourea and ammonia. Ammonia was shown to remove native oxides from the CIS surface [1].

The n-type CdS buffer layers on CIGS absorbers are used in order to form a heterojunction with the p-type CIGS and to protect the CIGS surface from ion damage during ZnO/ZnO:Al sputtering. CBD was reported to modify the surface of the CIS layer by forming an n-CdSe [1] or an n-$CuIn_xSe_y$ [2] intermediate layer, owing to strong reaction of the Cd with the CIS absorber. Schmid et al. [3] proposed a model that includes an n-type ordered vacancy chalcopyrite (OVC) layer between CIGS and CBD-CdS. These authors detected a buried heterojunction between p-CIGS and n-OVC directly by means of electron-beam-induced current measurements. In contrast to these results, Kylner et al. [4] found no evidence of an intermediate compound between CIGS and CBD-CdS. The role of the CdS buffer in the p–n junction formation will be treated further below.

Although the CBD process for CdS deposition is very attractive owing to high solar conversion efficiencies, for industrial production, an in-line vacuum deposition as, e.g., physical vapor deposition (PVD), is preferred. However, the highest efficiencies achieved by PVD-CdS buffer layers hardly exceed 13%. Always (e.g., [5]), a clearly poorer

* Corresponding author. Tel.: +41 1 633 21 26; fax: +41 1 633 11 05.
E-mail address: daniel.abou-ras@phys.ethz.ch (D. Abou-Ras).
[1] Now at: Università di Veronica, Cá Vignal 2, Strada Delle Grazie, 37134 Verona, Italy.
[2] Also at: Centre for Renewable Energy Systems and Technology (CREST), Department of Electronic and Electrical Engineering, Loughborough University, Leicestershire LE11 3TU, UK.

0040-6090/$ - see front matter © 2004 Elsevier B.V. All rights reserved.
doi:10.1016/j.tsf.2004.11.033

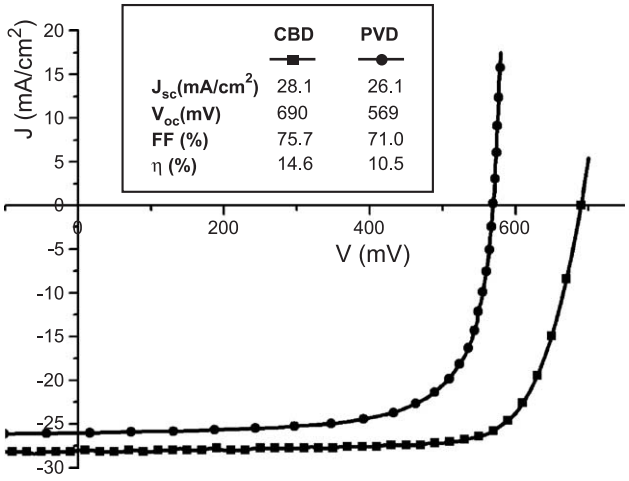

Fig. 1. *J–V* characteristics under AM1.5 illumination of solar cells with CBD-CdS and PVD-CdS buffer layers. Solar cells with CBD-CdS buffer layer always show higher efficiencies.

photovoltaic performance of solar cells with PVD-CdS buffer layers than of solar cells with CBD-CdS buffer layer was found. Recently, Romeo et al. [5] have published results from electrical investigations on solar cells with in situ and ex situ deposited PVD-CdS buffer layers and compared them with those of standard cells with CBD-CdS buffer layers.

In the present publication, investigations of structural and chemical properties of CBD- and PVD-CdS buffer layers and their interfaces with CIGS are presented. These results help to understand the reasons for the difference in the photovoltaic performance of solar cells produced by these two methods.

2. Experimental

Mo layers were sputtered on soda-lime glass (SLG) substrates, and CIGS layers were deposited by co-evaporation either at ETH Zurich, Switzerland or at the Center for Solar Energy and Hydrogen Research (ZSW), Stuttgart, Germany. CBD-CdS buffer layers were deposited by immersing the SLG/Mo/CIGS substrates in an aqueous bath containing cadmium acetate, ammonia and thiourea for 15 min at 70 °C. The deposition of PVD-CdS buffer layers was performed in a high-vacuum thermal evaporation system at 10^{-8} mbar and at a substrate temperature of 50 °C for 30 min. The solar cells were completed by the deposition of a rf-magnetron sputtered ZnO/ZnO:Al transparent bilayer.

Plan-view scanning electron microscopy (SEM) was performed on a Zeiss Gemini 1530 equipped with a field emission gun. Cross-section samples for transmission electron microscopy (TEM) were prepared by polishing, dimple grinding and finally ion milling using a GATAN precision ion polishing system. These samples were investigated by means of bright-field (BF-TEM), high-resolution (HR-TEM) and energy-filtered transmission electron microscopy (EF-TEM), and also by means of electron diffraction (ED) and energy-dispersive X-ray spectroscopy (EDX) using a FEI TECNAI F30 transmission electron microscope operated at 300 keV. EDX elemental mappings were measured on an area of 300×300 nm with a point-to-point distance of 6 nm using the scanning mode of the microscope. From these mappings, linear profiles were extracted. The linear profiles shown below were obtained by summing up several linear profiles from the elemental mappings, ensuring high accuracy of the measurement.

3. Results and discussion

In general, solar cells with CBD-CdS buffer layer yield efficiencies that are about 3–4% higher than those of solar cells with PVD-CdS buffer layer [5]. In Fig. 1, characteristics of two CIGS solar cells are displayed, both produced in the same run, yet one consisting of a CBD- and the other of a PVD-CdS buffer layer. The electrical properties, especially the open circuit voltage V_{oc}, differ significantly, probably owing to different interface and recombination properties.

In the plan-view SEM images in Fig. 2, small CdS grains are visible on top of large CIGS grains. PVD-CdS grains (b) are much larger than those of CBD-CdS (a). The size of the

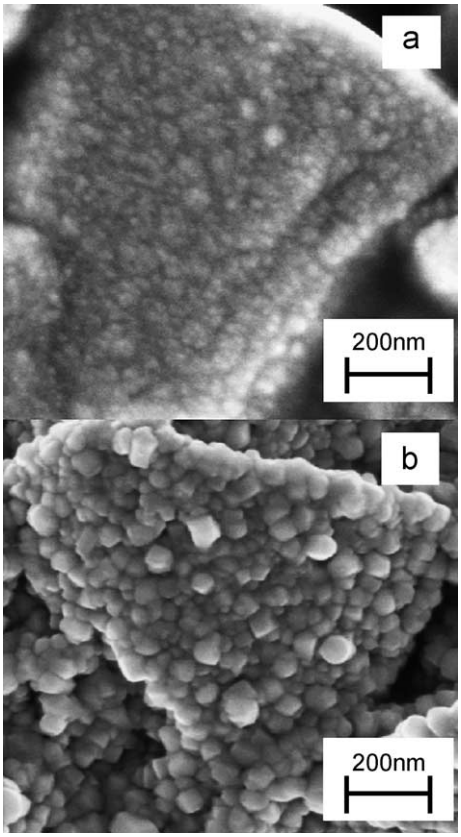

Fig. 2. (a) Plan-view scanning electron micrographs of CdS grains on large CIGS grains. PVD-CdS layers (b) showing significantly larger grain sizes than CBD-CdS (a).

PVD-CdS grains is approximately 70–80 nm, whereas the size of the CBD-CdS grains is too small to be determined from the SEM images.

In the BF-TEM images (Fig. 3), cross-sections of the interfaces between CIGS, CdS and ZnO are shown. Owing to different orientations with respect to the electron beam, specific grains of the same material may appear darker or brighter, as for, e.g., the CdS grains in Fig. 3a and b. By TEM as by means of SEM, the PVD-CdS grains (Fig. 3b) were found to be much larger than those of CBD-CdS (Fig. 3a): the PVD-CdS grain sizes from TEM agree well with the values obtained by means of SEM (about 70 nm). For the CBD-CdS layer, grain sizes of about 10–15 nm were determined. The CBD-CdS layer thickness was about 50 nm, whereas the PVD-CdS layer thickness was ca. 70 nm.

Fig. 4 shows the Cd signal from the CIGS/PVD-CdS/ZnO interface, obtained by means of EF-TEM. In contrast to prevailing views, the PVD-CdS layer shows a continuous coverage of the CIGS surface over a range of several micrometers, similar to the CBD-CdS coverage.

In Fig. 5, ED patterns for both the CIGS/CBD-CdS/ZnO interface (a) and the CIGS/PVD-CdS/CIGS interface (b) are shown. For the CBD-CdS layer (a), a hexagonal crystal structure was found. In general, CBD-CdS layers on CIGS, $CuInSe_2$ (CIS) or $CuGaSe_2$ (CGS) were reported to crystallize in both hexagonal (wurtzite, a=0.414 nm, c=0.671 nm [6]) and cubic (zincblende, a=0.582 nm [7]) crystal structures [2,8–12]. Furlong et al. [10] showed that the crystal structure of the CBD-CdS layer depends on the CIS substrate orientation. Nadenau et al. [11] found that the hexagonal and cubic crystal structure of CBD-CdS depends

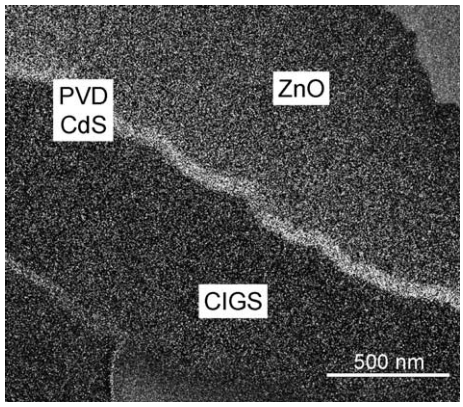

Fig. 4. Cd signal of the CIGS/PVD-CdS/ZnO interface region, obtained by means of energy-filtered transmission electron microscopy. The PVD-CdS layer shows a uniform conformal coverage of the CIGS surface.

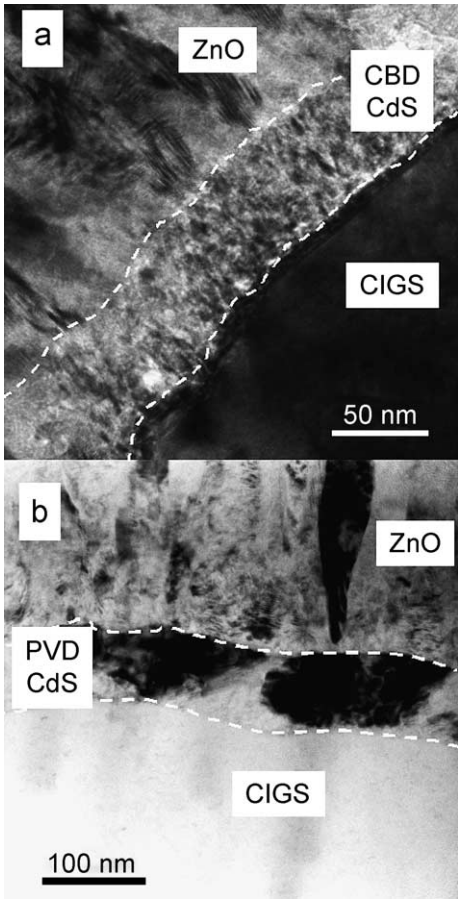

Fig. 3. Bright-field transmission electron micrograph of the CIGS/CBD-CdS/ZnO (a) and CIGS/PVD-CdS/ZnO (b) interfaces. Grain sizes are clearly larger for PVD-CdS than for CBD-CdS layers.

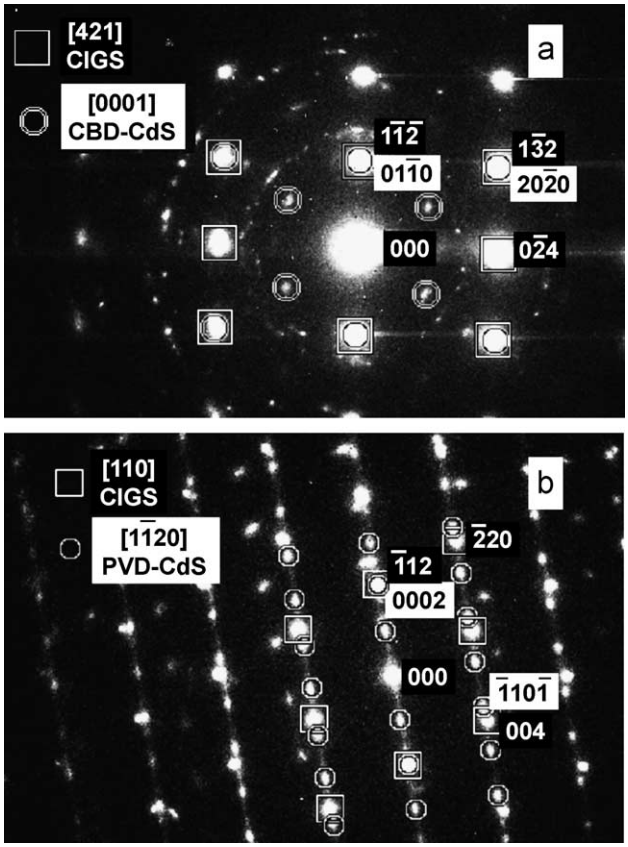

Fig. 5. Electron diffraction pattern for the CIGS/CBD-CdS/ZnO (a) and the CIGS/PVD-CdS/ZnO (b) interface. The growth of CBD-CdS on CIGS (a) is nearly coherent, whereas the growth of PVD-CdS on CIGS (b) is clearly incoherent.

on the substrate temperature during CBD. Thus, different CIGS deposition parameters and CBD-CdS recipes may lead to different CdS growth and crystal structure, and caution is advised not to generalize the detected crystal structure. Although wurtzite is the most stable crystal structure of CdS, the energy difference between wurtzite and zincblende is rather small [13], thus the transition may occur with high probability. Also, one has to take into account that the ED patterns of, e.g., $[111]_{cub}$ and $[0001]_{hex}$ CdS zone axes are difficult to distinguish, i.e. they might be misinterpreted.

A good lattice match of the CBD-CdS on the tetragonal CIGS layer is visible in Fig. 5a, since the reflections from CIGS-{112) and CdS-{01$\bar{1}$0) planes coincide, as well as the reflections from CIGS-{132) and CdS-{10$\bar{1}$0) planes.

For the PVD-CdS layer (Fig. 5b), a hexagonal crystal structure was also found. However, the lattice mismatch between PVD-CdS and CIGS is quite large; only CIGS-{112) and CdS-{0001) reflections coincide in the diffraction pattern. The difference in lattice (mis)match between CBD- and PVD-CdS may be due to the fact that the CBD-CdS layer is a mixture of CdS, Cd–OH, and Cd–O [4], which offers a range of lattice constants that apparently leads to a better lattice match to CIGS than the lattice constants of PVD-CdS.

In both ED patterns (Fig. 5), reflections from the hexagonal ZnO layer are also visible. For sample a, the ZnO grains show arbitrary orientations (diffraction rings), which can be expected from the small CBD-CdS grain size. For sample b, a preferential growth orientation in [11$\bar{2}$0] direction of the hexagonal ZnO on the PVD-CdS layer was found.

In Fig. 6a, a HR-TEM image of the CIGS/CBD-CdS interface corresponding to the ED pattern in Fig. 5a is shown. The marked lattice spacings in the CBD-CdS layer (ca. 0.37 nm) and in the CIGS layer (ca. 0.36 nm) agree well with the calculated values of hexagonal CdS-{10$\bar{1}$0) planes, 0.359 nm, and of CIGS-{112) planes, 0.366 nm (calculated from a=0.578 nm and c=1.16 nm [14]). As expected from the ED patterns, the micrograph shows good lattice match of CBD-CdS on CIGS.

The HR-TEM image of the CIGS/PVD-CdS interface in Fig. 6b reveals planar strains in the PVD-CdS, visible by a high density of defects, which arises from the compensation of the lattice mismatch. Defects generally contribute to recombination in the space charge region, which may lead to lower efficiencies.

Chemical properties of the CIGS/CBD-CdS (a) and CIGS/PVD-CdS (b) interfaces are shown by the linear composition profiles in Fig. 7. For reasons of clarity, the In and Ga signals were omitted, since they do not show any significant difference to the Se signal. Although the difference between the Cu and the Se signals, and also between the Cd and the S signals, is very small in Fig. 7a, the significance of these results can be assured by comparison of several linear profiles extracted from elemental mappings. In both diagrams (a and b), there is quite a clear cross-over of the Cu and Se signals with the Cd and S signals, and that is where the interface between CIGS and CdS was estimated (dashed lines).

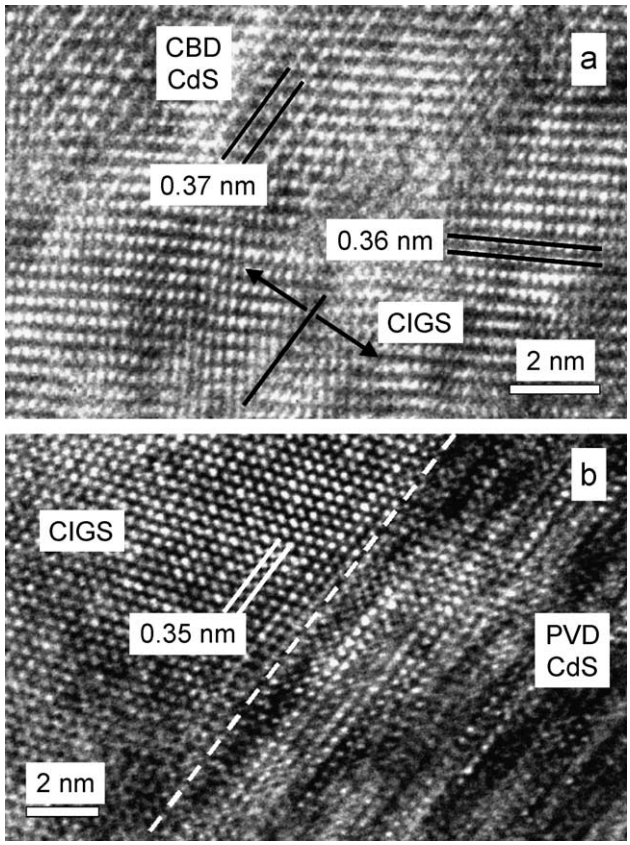

Fig. 6. High-resolution transmission electron micrograph of the CIGS/CBD-CdS (a) and of the CIGS/PVD-CdS (b) interface. In (a), the interface (see arrows) runs from the right-bottom corner (CIGS) to the left-top corner (CdS). In (b), the approximate position of the interface is given by the dashed line.

For both CIGS/CdS interfaces, Cu diffusion from the CIGS into the CdS layer is visible, since the Cu signal (■) decreases more slowly on the CdS side of the interface than the signal of Se. As mentioned by Bube [15], Cu doping of CdS increases its photoconductivity.

Only for the CBD-CdS sample (a), also a probable depletion of Cu and enrichment of Cd on the CIGS side of the interface is visible: the Cu signal is significantly lower than the Se signal, and the Cd signal (▲) decreases more slowly on the CIGS side of the interface than the S signal. Considering the probable Cu depletion in the case of the CBD-CdS/CIGS interface, one has to take into account that not all of the depleted Cu may diffuse from the CIGS into the CdS layer. Part of it will be dissolved in the CBD bath. Also, since CBD-CdS is not a stable compound, i.e. it consists of e.g. Cd–OH and Cd–O phases where Cd is not strongly bonded, Cd doping of the CIGS near-interface region is more likely in the case of CBD-CdS.

Compared with the CIGS/PVD-CdS interface (Fig. 7b), the CIGS/CBD-CdS (Fig. 7a) interface is not abrupt: it

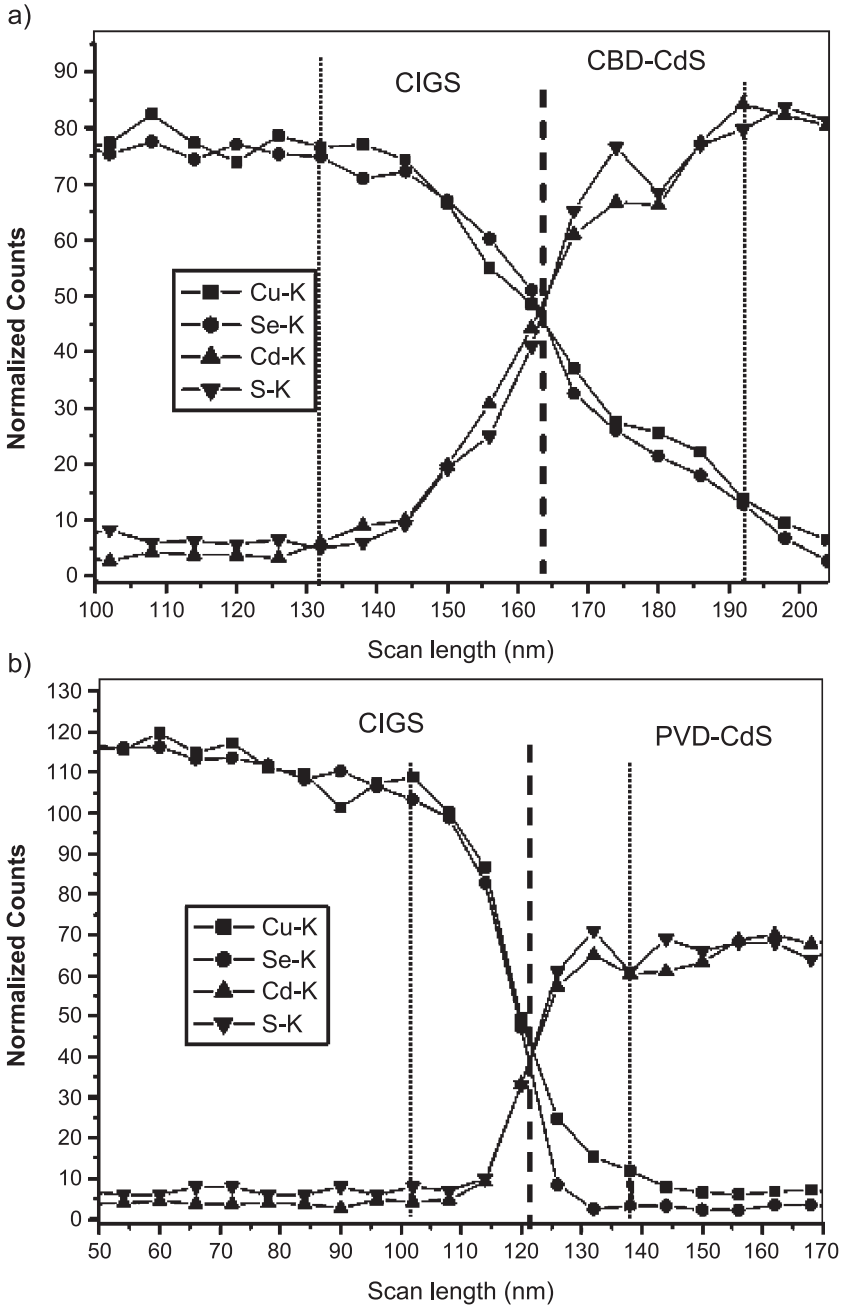

Fig. 7. Linear profiles over the CIGS/CdS interface extracted from elemental mappings, obtained by energy-dispersive X-ray spectrometry. For the CBD-CdS sample (a), there is Cu depletion and an increase of the Cd signal visible on the CIGS side of the interface, whereas no such behavior could be found for the PVD-CdS sample (b). The interface between CIGS and CdS is shown by the dashed line, whereas the dotted lines estimate the transition interfacial region. The Cu–K signals were normalized to the Se–K level on the CIGS side in order to provide an easier comparison.

shows quite a large transition interfacial region (dotted lines). It appears that Cu from the CIGS is incorporated into the CBD-CdS layer, depleting at the CIGS side of the interface, and that Cd diffuses from the CBD-CdS into the CIGS layer, occupying Cu vacancies in the near-interface region. Ramanathan et al. [16] discussed the influence of Cd on CIGS during the CBD process: owing to the similar ion radii of Cd^{2+} (0.97 Å) and Cu^{+} (0.96 Å), Cd ions may act as substitutional donors on Cu sites. By means of X-ray photo electron spectroscopy, these authors determined a Cd concentration of 20 at.% in the near-interface region on the CIGS side. Thus, this region may be inverted from p- to n-type, and a homojunction is formed. Nakada et al. [12] confirmed these results by means of EDX line scans, and Jiang et al. [17] identified this buried homojunction directly by means of scanning Kelvin probe microscopy. In addition, Wada et al. [18] showed that the treatment of the CIGS surface with a Cd^{2+} aqueous solution prior to PVD-CdS deposition improves the photovoltaic performance of the appropriate solar cells significantly.

The absence of Cd excess and Cu depletion on the CIGS side of the PVD-CdS/CIGS interface (Fig. 7b) and thus the probable absence of a homojunction may also lead to lower efficiencies in solar cells with PVD-CdS buffer layer.

4. Conclusion

Structural and chemical properties of CBD- and PVD-CdS/CIGS layers and interfaces were compared. PVD-CdS layers show much larger grain sizes than CBD-CdS layers, and also a higher defect density at the CIGS/PVD-CdS interface, owing to a larger lattice mismatch. These defects may affect on the photovoltaic performance. For the case of PVD-CdS, the interface to the CIGS is quite abrupt, whereas on the CIGS side of the CBD-CdS/CIGS interface Cu depletion and Cd enrichment may have occurred. Cu in CdS increases its photoconductivity, and Cd can occupy Cu vacancies. The results of the Cu and In interdiffusion provide an indication of an inversion of the near-interface region from p-type CIGS to n-type. The probable absence of this inversion in solar cells with PVD-CdS buffer layers is a possible reason for their lower efficiencies compared with solar cells with CBD-CdS buffer layer.

Acknowledgements

The authors are grateful to Peter Wägli, Electron Microscopy Center of the ETH Zurich, Switzerland, for the SEM measurements and to the ZSW, Stuttgart, Germany, for the supply of CIGS samples. This work was supported in part by the Swiss National Science Foundation, and also by the Swiss Federal Office of Science and Education for the EU projects PROCIS and NEBULES.

References

[1] J. Kessler, K.O. Velthaus, M. Ruckh, R. Laichinger, H.W. Schock, in: B.K. Das, S.N. Singh (Eds.), Proceedings of the 6th International Photovoltaic Science and Engineering Conference, New Delhi, India, February 10–14, 1992, p. 1005.
[2] D. Lincot, R. Ortega-Borges, J. Vedel, in: W. Palz, C. De Reyff, H. Kiess, P. Helm, L. Guimaraes, L. Guimarães (Eds.), Proceedings of the 11th European Photovoltaic Solar Energy Conference, Montreux, Switzerland, October 12–16, 1992, p. 870.
[3] D. Schmid, M. Ruckh, F. Grunwald, H.W. Schock, J. Appl. Phys. 73 (6) (1993) 2902.
[4] A. Kylner, J. Electrochem. Soc. 146 (5) (1999) 1816.
[5] A. Romeo, R. Gysel, S. Buzzi, D. Abou-Ras, D.L. Bätzner, D. Rudmann, F. Kurdesau, H. Zogg, A.N. Tiwari, Technical Digest of the 14th International Photovoltaic Science and Engineering Conference, Bangkok, Thailand, January 26–30, 2004, p. 705 (to be published in Sol. En. Mat. Sol. Cells).
[6] C. Palache, H. Berman, C. Frondel, The System of Mineralogy, 7th ed., Wiley, New York, 1958.
[7] R.J. Traill, R.W. Boyle, Am. Mineral. 40 (1955) 555.
[8] T. Wada, Sol. Energy Mater. Sol. Cells 49 (1997) 249.
[9] J.S. Chen, E. Kolawa, C.M. Garland, M.-A. Nicolet, Thin Solid Films 219 (1992) 183.
[10] M.J. Furlong, M. Froment, M.C. Bernard, R. Cortès, A.N. Tiwari, M. Krejci, H. Zogg, D. Lincot, J. Cryst. Growth 193 (1998) 114.
[11] V. Nadenau, D. Hariskos, H.W. Schock, M. Krejci, F.-J. Haug, A.N. Tiwari, H. Zogg, G. Kostorz, J. Appl. Phys. 85 (1) (1999) 534.
[12] T. Nakada, Thin Solid Films 361–362 (2000) 345.
[13] C.-Y. Yeh, Z.W. Lu, S. Froyen, A. Zunger, Phys. Rev., B 46 (16) (1992) 10086.
[14] K.S. Knight, Mater. Res. Bull. 27 (2) (1992) 161.
[15] R.H. Bube, Photoconductivity in Solids, Wiley, New York, 1960.
[16] K. Ramanathan, R. Noufi, J. Granata, J. Webb, J. Keane, Sol. Energy Mater. Sol. Cells 55 (1998) 15.
[17] C.-S. Jiang, F.S. Hasoon, H.R. Moutinho, H.A. Al-Thani, M.J. Romero, M.M. Al Jassim, Appl. Phys. Lett. 82 (1) (2003) 127.
[18] T. Wada, S. Hayashi, Y. Hashimoto, S. Nishiwaki, T. Sato, T. Negami, M. Nishitani, in: J. Schmid, H.A. Ossenbrink, P. Helm, H. Ehmann, E.D. Dunlop (Eds.), Proceedings of the 2nd World Conference and Exhibition on Photovoltaic Energy Conversion, Vienna, Austria, July 6–10, 1998, p. 403.